Proceedings of ALGORITMY 2005
pp. 1–11

FINITE ELEMENT SIMULATION OF A DROPLET IMPINGING A HORIZONTAL SURFACE

SASHIKUMAAR GANESAN* AND LUTZ TOBISKA†

Abstract. This paper presents the shape deformation of a single two dimensional spherical liquid droplet on a horizontal surface. The mathematical model can be defined by the time-dependent Navier-Stokes equations in a time-dependent domain. The model has to be completed by the free boundary condition on the fluid-gas interface and the Navier-slip boundary condition on the fluid-solid interface, respectively. A second order finite element discretization in space is combined with a fractional θ-scheme to solve this free surface problem. The Arbitrary Lagrangian Eulerian method is used to handle the time dependent domain. Replacing the curvature term on the free surface by the Laplace-Beltrami operator we are able to include the contact angle explicitly in the finite element formulation. The numerical results show that the shape deformation is influenced by the impact velocity, the droplet diameter, the surface tension and material properties.

Key words. Navier-Stokes equation, finite elements, ALE approach, Laplace-Beltrami operator

AMS subject classifications. 65M60, 65M50, 76D05, 76D45

1. Introduction. Deformation of a droplet on a horizontal surface has been studied for over a century [9] not only of physical interest but also due to its industrial applications such as spray cooling, spray forming, spray coating, ink-jet printing, fuel injecting and etc. Fluid flow simulation of these type of models are more challenging than the CFD simulation in a fixed domain with given velocities at the boundaries because of the no-slip condition on solid surface, deforming domains and dynamic wetting line. Each of the above aspect is complicated.

Using the usual no-slip boundary condition on the solid-liquid interface leads to an unsatisfactory model, because the conventional fluid mechanical analysis indicates that exceedingly high stress occur in the neighbourhood of the contact line [7, 11, 12, 19]. Different versions of boundary conditions are discussed in [8]. Among those, Navier-slip condition is widely accepted. The difficulty in this condition is to provide an appropriate value for the slip coefficient. Often, it is considered as a constant but more complicated nonlinear forms are also used in molecular dynamics, see e.g. [20]. We replace the curvature term on the free surface by the Laplace-Beltrami operator. This technique was successfully applied in the finite element context, see e.g [1, 2, 15]. By using this relation we are able to take into consideration the contact angle in the finite element model which is quite important for including surface properties of the solid wall.

For handling time dependent domains, different techniques has been proposed in the literature. The oldest approach is the Marker and Cell (MAC) method, in which marker particles are used to identify each phase. In the Volume of Fluid (VOF) method, a marker function representing the fraction of the fluid in a cell is used. In the considered case of application a precise implementation of the force balance at the free surface including in particular the influence of surface tension is important. It

*Institut für Analysis und Numerik, Otto-von-Guericke-Universität Magdeburg, D-39106 Magdeburg. (ga.sashikumaar@mathematik.uni-magdeburg.de).

†Institut für Analysis und Numerik, Otto-von-Guericke-Universität Magdeburg, D-39106 Magdeburg.(lutz.tobiska@mathematik.uni-magdeburg.de).

is difficult to implement the corresponding boundary condition within the framework of the MAC and VOF method due to a missing sharp interface reconstruction. A widely used and very flexible method is the Level Set method (LS) [18], in which, the interface is represented as an implicit smooth level set function. It allows topological changes of the domain but the discretization of the equation to advect the level set function increases the computational cost and causes numerical errors. These errors influence the mass conservation even though the incompressibility condition is taken into account. To avoid the problems described above we use alternatively the Arbitrary Lagrangian Eulerian approach (ALE) [15, 16]. In this method the grid points can move independent of the fluid motion. In particular, the inner grid points can be displaced in an arbitrary prescribed way to get a proper mesh quality.

On the real surface we have to face the contact angle hysteresis. Let the advancing contact angle θ_{adv} be the angle just before the spreading starts and the receding contact angle θ_{rec} be the angle just before the recoiling starts. Usually θ_{adv} is significantly higher than θ_{rec}. The difference is called the contact angle hysteresis. Various explanations for the occurrence of the hysteresis have been given in the literature [5].

The paper is organised as follows. Section 2 presents the overview of the problem and the governing equations of the model. Section 3 deals with the time discretization schemes, finite element formulation, ALE approach to handle the time-dependent domains, automatic mesh update and remeshing schemes. Results of numerical tests are summarised in Section 4.

2. Mathematical model.

2.1. Model problem. We consider the two-dimensional liquid droplet impinging on a horizontal solid surface, starting at an instant $t = 0$ when the droplet comes into contact with the solid surface. We proceed until the prescribed time is reached or the droplet comes to rest after the spreading and recoiling processes completed.

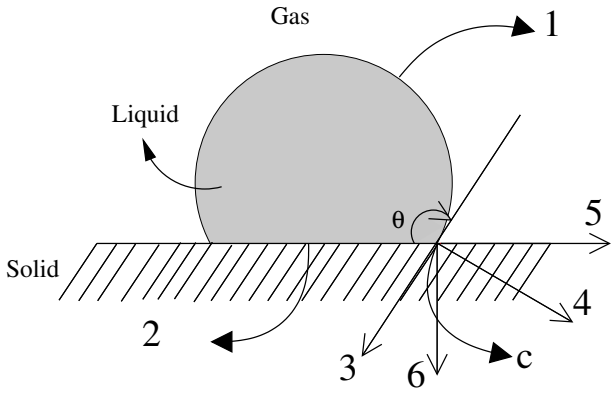

FIG. 2.1. *Droplet Deformation.*

In Fig.2.1, (1) and (2) are the fluid-gas (Γ_F) and fluid-solid (Γ_S) interfaces, respectively, c is the dynamic wetting point. (3), (4) are unit tangential (τ_F), unit outward normal (ν_F) vectors on Γ_F, and (5), (6) are unit tangential (τ_S), unit outward normal (ν_S) vectors on Γ_S.

2.2. Governing Equations. The two-dimensional fluid flow within the considered bounded domain $\Omega(t)$, $t \in [0, T]$, is governed by the two-dimensional time-

dependent incompressible Navier-Stokes equations

$$\begin{aligned} \frac{\partial \mathbf{u}}{\partial t} + (\mathbf{u}\cdot\nabla)\mathbf{u} - \frac{1}{\rho}\nabla\cdot\sigma(\mathbf{u},p) &= \mathbf{f} \quad \text{in } \Omega(t) \\ \nabla\cdot\mathbf{u} &= 0 \quad \text{in } \Omega(t) \end{aligned} \tag{2.1}$$

where $\mathbf{u} = (u_1, u_2)$ denote the velocity, p the pressure, ρ the density, and $\mathbf{f} = (\mathbf{f_1}, \mathbf{f_2}) = (\mathbf{0}, -\mathbf{g})$ the body force with the gravity constant g. The stress tensor σ is given by

$$\sigma(\mathbf{u},p) = 2\mu D(\mathbf{u}) - p\mathbf{I}, \qquad D(\mathbf{u}) = \frac{1}{2}(\nabla\mathbf{u} + \nabla\mathbf{u}^T) \tag{2.2}$$

with the dynamic viscosity μ and the identity tensor $\mathbf{I}$.

2.3. Initial and Boundary Conditions. At time $t = 0$ we assume that the droplet is of spherical shape with radius r_0

$$\Omega(0) = \left\{x \in \mathbb{R}^2 \,:\, x_1^2 + (x_2 - r_0)^2 < r_0^2\right\}$$

and has the initial velocity

$$\mathbf{u}(0) = (0, -u_0) \tag{2.3}$$

where u_0 denotes the pre impact velocity. Along the liquid-gas interface Γ_F the boundary conditions

$$\nu_F \cdot \sigma_{\nu_F} = -(\gamma\kappa + p_0), \qquad \tau_F \cdot \sigma_{\nu_F} = 0 \tag{2.4}$$

are applied. Here, σ_{ν_F} denotes the normal component of the stress tensor (with respect to Γ_F), γ the surface tension, κ the curvature, and p_0 the atmospheric pressure. Further, the kinematic boundary condition

$$\mathbf{u}\cdot\nu_F = V_{\Gamma_F} \qquad \text{on } \Gamma_F(t) \tag{2.5}$$

holds, i.e the normal component of the velocity at the liquid-gas interface corresponds to the interface velocity V_{Γ_F}. Along the liquid-solid interface Γ_S the Navier-slip boundary condition

$$\mathbf{u}\cdot\nu_S = 0 \qquad \mathbf{u}\cdot\tau_S = -\frac{1}{\beta}(\tau_s \cdot \sigma_{\nu_s}) \tag{2.6}$$

is used, where σ_{ν_s} is the normal component of the stress tensor (with respect to Γ_S) and β denotes the so called slip coefficient. For the simplicity we consider it as a constant.

2.4. Dimensionless Form. We choose as the reference length d_0, as the reference velocity u_0, i.e., the diameter and the pre impact velocity of the droplet at $t = 0$, respectively. Introducing the dimensionless quantities

$$\tilde{\mathbf{u}} = \frac{\mathbf{u}}{u_0}, \quad \tilde{p} = \frac{p - p_0}{\rho u_0^2}, \quad \tilde{t} = \frac{t u_0}{d_0}, \quad \tilde{x} = \frac{x}{d_0}, \quad \tilde{\sigma} = \frac{\sigma}{\rho u_0^2}$$

and omitting the tilde afterwards, we obtain the problem in the dimensionless form

$$\begin{aligned} &\frac{\partial \mathbf{u}}{\partial t} + (\mathbf{u}\cdot\nabla)\mathbf{u} - \nabla\cdot\sigma(\mathbf{u},p) = \mathbf{f}, \qquad \nabla\cdot\mathbf{u} = \mathbf{0}, && \text{in } \Omega(t) \\ &\tau_F \cdot \sigma_{\nu_F} = 0, \qquad \nu_F \cdot \sigma_{\nu_F} = -\frac{1}{We}\kappa && \text{on } \Gamma_F \\ &\mathbf{u}\cdot\nu_S = 0, \qquad \tau_s \cdot \sigma_{\nu_s} = -\frac{\beta}{\rho\mathbf{u}_0}\mathbf{u}\cdot\tau_s && \text{on } \Gamma_S \end{aligned} \tag{2.7}$$

where the stress tensor is given by

$$\sigma(\mathbf{u},p) = \frac{2}{Re}D(\mathbf{u}) - p\mathbf{I}, \tag{2.8}$$

and

$$Re = \frac{\rho u_0 d_0}{\mu}, \quad We = \frac{\rho u_0^2 d_0}{\gamma}, \quad Fr = \frac{u_0^2}{d_0 g} \tag{2.9}$$

denote the Reynolds number, the Weber number, and the Froude number. Now, the initial condition becomes $\mathbf{u}(0) = (0,-1)$ and the right hand side $\mathbf{f} = (0,-Fr^{-1})$.

3. Numerical Schemes. The starting point of formulating a finite element method is a weak formulation of the problem (2.7). We discretize the weak problem in time and then in space.

3.1. Weak Formulation. In this section we use the short notation Ω for $\Omega(t)$. Let $L^2(\Omega)$ and $H^m(\Omega)$, $m \geq 1$ be the usual Lebesgue and Sobolev spaces. To include the boundary condition $\mathbf{u}\cdot\nu_S = 0$ on Γ_S in the weak formulation we define

$$V := \{\mathbf{v} \in H^1(\Omega)^2 : \mathbf{v}\cdot\nu_S = 0\}$$

and $Q = L^2(\Omega)$ as the velocity and pressure spaces, respectively.

The weak formulation is obtained by multiplying (2.7) with a test function $\mathbf{v} \in V$ and integrating over Ω. We restrict our derivation on the stress tensor term and handle the remaining terms in the usual way. Applying the Gaussian theorem we get for the stress tensor

$$\begin{aligned}
&-\textstyle\int_\Omega \nabla\cdot\sigma(\mathbf{u},p)\cdot\mathbf{v}\,dx \\
&\quad = \textstyle\int_\Omega \sigma(\mathbf{u},p) : \nabla\mathbf{v}\,dx - \int_\Gamma \mathbf{v}\cdot\sigma(\mathbf{u},p)\nu\,d\gamma \\
&\quad = \textstyle\int_\Omega \frac{1}{2}\sigma(\mathbf{u},p) : \nabla\mathbf{v}\,dx + \int_\Omega \frac{1}{2}\sigma^T(\mathbf{u},p) : \nabla\mathbf{v}\,dx - \int_\Gamma \mathbf{v}\cdot\sigma(\mathbf{u},p)\nu\,d\gamma \\
&\quad = \textstyle\int_\Omega \sigma(\mathbf{u},p) : \mathbf{D}(\mathbf{v})\,dx - \int_\Gamma \mathbf{v}\cdot\sigma(\mathbf{u},p)\nu\,d\gamma \\
&\quad = \frac{2}{Re}\displaystyle\int_\Omega \mathbf{D}(\mathbf{u}) : \mathbf{D}(\mathbf{v})\,dx - \int_\Omega p\nabla\cdot\mathbf{v}\,dx - \int_\Gamma \mathbf{v}\cdot\sigma(\mathbf{u},p)\nu\,d\gamma\,.
\end{aligned}$$

Note that we have used the symmetry of the stress tensor $\sigma(\mathbf{u},p)$. Now we split the boundary integral into integral over Γ_S and Γ_F, i.e.,

$$\textstyle\int_\Gamma \mathbf{v}\cdot\sigma(\mathbf{u},p)\nu\,d\gamma \;=\; \int_{\Gamma_S} \mathbf{v}\cdot\sigma(\mathbf{u},p)\nu_S\,d\gamma_S + \int_{\Gamma_F} \mathbf{v}\cdot\sigma(\mathbf{u},p)\nu_F\,d\gamma_F\,. \tag{3.1}$$

For the first term on the right hand side in (3.1) we decompose $\mathbf{v}$ as $\mathbf{v} = (\mathbf{v}\cdot\nu_S)\nu_S + (\mathbf{v}\cdot\tau_S)\tau_S$, use (2.6) and $\mathbf{v}\in V$, to get

$$\begin{aligned}
&\textstyle\int_{\Gamma_S} \mathbf{v}\cdot\sigma(\mathbf{u},p)\nu_S\,d\gamma_S \\
&\quad = \textstyle\int_{\Gamma_S} (\mathbf{v}\cdot\tau_S)\tau_S\cdot\sigma(\mathbf{u},p)\nu_S\,d\gamma_S + \int_{\Gamma_S} (\mathbf{v}\cdot\nu_S)\nu_S\cdot\sigma(\mathbf{u},p)\nu_S\,d\gamma_S \\
&\quad = -\textstyle\int_{\Gamma_S} \beta(\mathbf{u}\cdot\tau_S)(\mathbf{v}\cdot\tau_S)\,d\gamma_S\,.
\end{aligned} \tag{3.2}$$

For the second term in (3.1) we decompose $\mathbf{v}$ as $\mathbf{v} = (\mathbf{v}\cdot\nu_F)\nu_F + (\mathbf{v}\cdot\tau_F)\tau_F$ and use (2.4), to get

$$\begin{aligned}
&\textstyle\int_{\Gamma_F} \mathbf{v}\cdot\sigma(\mathbf{u},p)\nu_F\, d\gamma_F \\
&\quad = \textstyle\int_{\Gamma_F}(\mathbf{v}\cdot\tau_F)\tau_F\cdot\sigma(\mathbf{u},p)\nu_F\, d\gamma_F + \int_{\Gamma_F}(\mathbf{v}\cdot\nu_F)\nu_F\cdot\sigma(\mathbf{u},p)\nu_F\, d\gamma_F \\
&\quad = -\textstyle\int_{\Gamma_F}(\mathbf{v}\cdot\nu_F)\frac{\kappa}{We}\, d\gamma_F.
\end{aligned} \tag{3.3}$$

Now we replace the curvature term $-\kappa\nu_F$ by the Laplace-Beltrami operator and integrate it by parts

$$\begin{aligned}
-\textstyle\int_{\Gamma_F}\mathbf{v}\cdot\nu_F\frac{\kappa}{We}\, d\gamma_F &= \frac{1}{We}\int_{\Gamma_F}\underline{\Delta} id_{\Gamma_F}\cdot\mathbf{v}\, d\gamma_F \\
&= \frac{1}{We}\left(-\int_{\Gamma_F}\underline{\nabla} id_{\Gamma_F} : \underline{\nabla}\mathbf{v}\, d\gamma_F + (\gamma_\nu\cdot\underline{\nabla} id_{\Gamma_F})\cdot\mathbf{v}\Big|_{c_r}^{c_l}\right) \\
&= \frac{1}{We}\left(-\int_{\Gamma_F}\underline{\nabla} id_{\Gamma_F} : \underline{\nabla}\mathbf{v}\, d\gamma_F + \gamma_\nu\cdot\mathbf{v}\Big|_{c_r}^{c_l}\right)
\end{aligned}$$

since $\gamma_\nu\cdot\underline{\nabla} id_{\Gamma_F} = \gamma_\nu$. Here, γ_ν denotes the outer normal at the wetting points c_r and c_l with respect to Γ_F. We decompose $\mathbf{v}$ in the second term as $\mathbf{v} = (\mathbf{v}\cdot\nu_S)\nu_S + (\mathbf{v}\cdot\tau_S)\tau_S$ and use the condition $\mathbf{v}\cdot\nu_S = 0$ on Γ_S to obtain

$$\begin{aligned}
-\textstyle\int_{\Gamma_F}\mathbf{v}\cdot\nu_F\frac{\kappa}{We}\, d\gamma_F &= \frac{1}{We}\left(-\int_{\Gamma_F}\underline{\nabla} id_{\Gamma_F} : \underline{\nabla}\mathbf{v}\, d\gamma_F + (\gamma_\nu\cdot\tau_S)(\mathbf{v}\cdot\tau_S)\Big|_{c_r}^{c_l}\right) \\
&= \frac{1}{We}\left(-\int_{\Gamma_F}\underline{\nabla} id_{\Gamma_F} : \underline{\nabla}\mathbf{v}\, d\gamma_F + \cos(\theta)\ \mathbf{v}\cdot\tau_S\Big|_{c_r}^{c_l}\right)
\end{aligned} \tag{3.4}$$

where the restriction of the mapping $id_{\Gamma_F} : \mathbb{R}^2 \to \mathbb{R}^2$ onto Γ_F is the identity.

Now the weak form of (2.7) reads:

Find $(\mathbf{u},p) = (\mathbf{u}(t),p(t)) \in V\times Q$ such that for all $(\mathbf{v},q)\in V\times Q$ such that

$$\begin{aligned}
\left(\frac{\partial\mathbf{u}}{\partial t},\mathbf{v}\right) + a_D(\mathbf{u},\mathbf{v}) + b(\mathbf{u},\mathbf{u},\mathbf{v}) + e(\mathbf{u},\mathbf{v}) + d(\mathbf{u},\mathbf{v}) - c(p,\mathbf{v}) &= (f,\mathbf{v}) + h(\theta,\mathbf{v}) \\
c(q,\mathbf{u}) &= 0
\end{aligned} \tag{3.5}$$

where

$$\begin{aligned}
a_D(\mathbf{u},\mathbf{v}) &= \frac{2}{Re}\int_\Omega \mathbf{D}(\mathbf{u}) : \mathbf{D}(\mathbf{v})\, dx, & b(\hat{\mathbf{u}},\mathbf{u},\mathbf{v}) &= \textstyle\int_\Omega(\hat{\mathbf{u}}\cdot\nabla)\mathbf{u}\cdot\mathbf{v}\, dx, \\
e(\mathbf{u},\mathbf{v}) &= \frac{1}{We}\int_{\Gamma_F}\underline{\nabla} id_{\Gamma_F} : \underline{\nabla}\mathbf{v}\, d\gamma_F, & d(\mathbf{u},\mathbf{v}) &= \textstyle\frac{\beta}{\rho\mathbf{u}_0}\int_{\Gamma_S}(\mathbf{u}\cdot\tau)(\mathbf{v}\cdot\tau)\, d\gamma_S, \\
c(q,\mathbf{v}) &= \textstyle\int_\Omega q\nabla\cdot\mathbf{v} & (f,\mathbf{v}) &= \textstyle\int_\Omega f\cdot\mathbf{v}\, dx, \\
h(\theta,\mathbf{v}) &= \frac{1}{We}\cos(\theta)\ \mathbf{v}\cdot\tau_S\Big|_{c_r}^{c_l}.
\end{aligned}$$

Remark : **3.1.1** For a contact angle $\theta = \pi/2$ the linear form $\mathbf{v} \to h(\theta, \mathbf{v})$ vanishes and (2.7) is well defined. In all other cases $\mathbf{v}$ has to belong to $H^{1+\varepsilon}$, $\varepsilon > 0$, to guarantee the continuity of that linear form.

3.2. Temporal discretization.

3.2.1. Time stepping techniques. Let $0 = t_0 < t_1 < \cdots < t_N = T$ be a decomposition of the considered time interval. Since our domain $\Omega = \Omega(t)$ is time-dependent, the corresponding spaces V, Q, depend also on time. We shall use the notation V^n and Q^n to indicate this dependency. Define $\tau_n = t_{n+1}$ - t_n. We (semi-) discretize (3.5) in time by using the integration formula

$$\int_{t_n}^{t_{n+1}} \varphi(t)\, dt \approx \tau_n[(1-\vartheta)\varphi(t_n) + \vartheta\varphi(t_{n+1})].$$

This results in the sequence of generalised stationary Navier-Stokes problems:

Given $\mathbf{u}^n \in V^n$, $p^n \in Q^n$, find $\mathbf{u} = \mathbf{u}^{n+1} \in V^{n+1}$, p $= p^{n+1} \in Q^{n+1}$ such that

$$\begin{aligned} [1 + \vartheta\ \mathrm{N}(\mathbf{u})](\mathbf{u}, \mathbf{v}) \text{ - } \tau_n(p, \nabla\cdot\mathbf{v}) &= [1 \text{ - } (1-\vartheta)N(\mathbf{u}^n)](\mathbf{u}^n, \mathbf{v}) \\ &\quad + \tau_n(f^{n+1}, \mathbf{v}) + c(\theta, \mathbf{v}) \\ (\nabla\cdot\mathbf{u},\, \mathrm{q}) &= 0. \end{aligned} \tag{3.6}$$

Choosing ϑ as 0, 1, or 0.5, we obtain the forward Euler, the backward Euler or the Crank- Nicolson scheme, respectively. Here and in the following, we use the compact representation

$$N(\hat{\mathbf{u}})(\mathbf{u}, \mathbf{v}) = a_D(\mathbf{u}, \mathbf{v}) + b(\hat{\mathbf{u}}, \mathbf{u}, \mathbf{v}) + e(\mathbf{u}, \mathbf{v}) + d(\mathbf{u}, \mathbf{v}) \tag{3.7}$$

3.2.2. Fractional ϑ scheme. The Euler schemes are of first order and the Crank-Nicolson scheme is of second order. Unfortunately, the latter one is not strongly A-stable. That means this scheme may lead to numerical oscillations in the problem with rough initial data or boundary conditions. An alternative to the one-step ϑ schemes is the fractional step ϑ scheme proposed first in [4] as an operator splitting scheme. It combines three first order one step schemes in a clever way to get a second order strongly A-stable scheme. For more details we refer to [15, 17, 21].

Let $\vartheta = 1\text{-}\ \frac{\sqrt{2}}{2}$, $\vartheta' = 1 - 2\vartheta$, $\eta = \dfrac{\vartheta'}{1-\vartheta}$ and $\eta' = 1 - \eta$. We split each τ_n into three subintervals as (t_n, t_{n_1}), (t_{n_1}, t_{n_2}) and (t_{n_2}, t_{n+1}). Where $t_{n_1} = t_n + \tau_n\vartheta$ and $t_{n_2} = t_{n+1} - \tau_n\vartheta$. The fractional ϑ scheme for (3.5) in the time interval (t_n, t_{n+1}) consists of three steps.

Step 1. Find $\mathbf{u} = \mathbf{u}^{n+\tau_n\vartheta}, p = p^{n+\tau_n\vartheta}$ in $V^{n+\tau_n\vartheta} \times Q^{n+\tau_n\vartheta}$ such that for all $(\mathbf{v}, q)$ in $V^{n+\tau_n\vartheta} \times Q^{n+\tau_n\vartheta}$

$$\begin{aligned} [1 + \theta_1\ \mathrm{N}(\mathbf{u})](\mathbf{u}, \mathbf{v})|_{\Omega(t_n)} \text{ - } \vartheta\tau_n(p, \nabla\cdot\mathbf{v}) &= [1 \text{ - } \theta_2 N(\mathbf{u}^n)](\mathbf{u}^n, \mathbf{v}) \\ &\quad + \vartheta\tau_n(f^{n+\tau_n\vartheta}, \mathbf{v}) + \vartheta\tau_n c(\theta, \mathbf{v}) \\ (\nabla\cdot\mathbf{u},\, \mathrm{q}) &= 0 \end{aligned} \tag{3.8}$$

where $\theta_1 = \tau_n\vartheta\eta$, $\theta_2 = \tau_n\vartheta\eta'$. Similarly in Step 2 and 3 we find $(\mathbf{u}_{n+1-\tau_n\vartheta}, p_{n+1-\tau_n\vartheta})$ and $(\mathbf{u}_{n+1}, p_{n+1})$ belonging to the spaces defined on the domains at time t_{n_2} and t_{n+1}. The difficulty in the time discretization (3.8) is that we are looking the solution defined on $\Omega(t_{n_1})$ from a solution defined on $\Omega(t_n)$. In the next subsection we overcome this difficulty by using Arbitrary Lagrangian Eulerian method.

3.2.3. Arbitrary Lagrangian Eulerian (ALE) Approach. Let A_t be a family of mappings, which at t ∈ [0,T] maps a point $Y \in \Omega(t_n)$ of a reference domain onto the point x of the current domain $\Omega(t_{n+1})$:

$$A_{t_{n+1}} : \Omega(t_n) \to \Omega(t_{n+1}), \quad A_{t_{n+1}}(Y) = x(Y, t_{n+1}). \tag{3.9}$$

We assume that A_{t_n} is homeomorphic for $n = 1, 2, \ldots$, that is A_{t_n} is invertible with continuous image. Further, we assume that the mapping is differentiable almost everywhere in [0, T]. Let $Y \in \Omega(t_n)$ be ALE coordinate and x= $x(Y, t_{n+1})$ be spatial or Eulerian coordinate. In order to explain the ALE approach we consider for simplicity a first order time evolution problem.

Find $\mathbf{u} \in V^{n+1}$ such that

$$\frac{\partial \mathbf{u}}{\partial t} + L(\mathbf{u}) = 0 \tag{3.10}$$

with appropriate boundary conditions. Here, L denotes a differential operator. To find an equivalent form for $\mathbf{u}^{n+1} \circ A_{t_{n+1}}$, we apply the chain rule to the time derivative in the ALE frame and obtain

$$\begin{aligned} \frac{\partial \mathbf{u}}{\partial t}\Big|_Y &= \frac{\partial \mathbf{u}}{\partial t}\Big|_x + \frac{\partial x}{\partial t}\Big|_Y \cdot \nabla_x \mathbf{u} \\ &= \frac{\partial \mathbf{u}}{\partial t}\Big|_x + \mathbf{w}^n \cdot \nabla_x \mathbf{u} \end{aligned} \tag{3.11}$$

We see that using the ALE formulation we are getting an additional convective term due to the domain movement which requires the domain velocity $\mathbf{w}$ in each time step. For more details on derivation and different forms we refer to [16].

For (3.6) the ALE formulation can be obtain in the same way. The only change is an additional convective term, i.e., we have to replace (3.7) by

$$N(\hat{\mathbf{u}})(\mathbf{u}, \mathbf{v}) = a_D(\mathbf{u}, \mathbf{v}) + b((\hat{\mathbf{u}} - \mathbf{w}^n), \mathbf{u}, \mathbf{v}) + e(\mathbf{u}, \mathbf{v}) + d(\mathbf{u}, \mathbf{v}) \tag{3.12}$$

3.2.4. Handling the curvature term. The boundary integral term $e(\mathbf{u}, \mathbf{v})$ in (3.5) can be treated as fully explicit, fully implicit or semi-implicit. Numerical experiments [1] with the explicit form show that the resulting scheme is only conditionally stable. The implicit form is too complicated because we need in advance the domain $\Omega(t_{n+1})$ which is unknown. So, we consider the semi-implicit form as proposed in [1, 15]

$$\int_{\Gamma_F(t_n)} \underline{\nabla} id_{\Gamma_F(t_{n+1})} : \underline{\nabla}\mathbf{v}\, d\gamma_F \approx \int_{\Gamma_F(t_n)} (\underline{\nabla} id_{\Gamma_F(t_n)} + \tau_n \underline{\nabla}\mathbf{u}^{n+1}) : \underline{\nabla}\mathbf{v}\, d\gamma_F$$

Now, only the term $\int_{\Gamma_F(t_n)} \underline{\nabla}\mathbf{u}^{n+1} : \underline{\nabla}\mathbf{v}\, d\gamma_F$ is unknown and will be shifted to the left hand side of the equation leading to a better stability due to its symmetry and positive semi-definiteness. In [1] the new position X^{n+1} of the boundary nodes are obtained by moving it in the normal direction as

$$X^{n+1} = X^n + \tau_n(\nu_F \cdot \mathbf{u}^{n+1}(X^n))\nu_F. \tag{3.13}$$

This may not be true in the neighbourhood of the wetting points. Alternatively a generalised elevation equation for free boundary displacement was used in [3]. In this case the update form is given by

$$X^{n+1} = X^n + \Phi(X^n)\mathbf{e}(X^n) \tag{3.14}$$

where $\Phi(X^n)$ and $\mathbf{e}(X^n)$ are the displacement and prescribed direction of X^n. In our numerical calculation we used the simple form that if $\mathbf{u}^{n+1}$ is known then we get the new position of the boundary nodes as

$$X^{n+1} = X^n + \tau_n \mathbf{u}^{n+1}(X^n). \tag{3.15}$$

For simplicity, the second term in the equation (3.4) has been discretized explicitly.

3.3. Discretization in space by Finite elements. Theoretical results for finite element discretizations of (2.1) in a fixed domain $\Omega = \Omega(t)$ for Dirichlet type boundary conditions $\mathbf{u} \mid_{\partial\Omega} = 0$ can be found in many textbooks, see for example [10]. To guarantee the stability and high accuracy we prefer inf-sup stable elements of at least second order. We prefer triangular elements, the obvious reason is that they will approximate the complex and time dependent domains more accurately than quadrilateral elements. The popular triangular element is the Taylor Hood element, i.e., continuous piecewise quadratic approximations for the velocity and continuous piecewise linear pressures. Using continuous elements for the pressure space approximation we can guarantee the mass conservation only over patches of elements. Discontinuous elements provides the mass conservation locally i.e., element by element. Therefore, we prefer the discontinuous piecewise linear element for approximating the pressure space. In order to satisfy the inf-sup condition we need to add to the usual piecewise quadratics a cubic bubble function. The inf-sup stability of this element has been shown in [6].

3.4. Mesh update and remeshing. As we discussed in Section 3.2.4 we get the new position of the boundary nodes in each time step. According to that we have to move the interior nodes also. We can achieve this by remeshing the domain according to the new boundary points and project the solution from the old domain to the new one in each time step. This procedure obviously increases the computational costs and also causes projection errors. To avoid as much as possible remeshing, we combine the elastic solid technique to find the new position of the interior nodes and remesh the domain only when the distortion of the finite element become exceedingly large. For elastic solid technique we follow the ideas given by Matthies [15]. We remesh the domain if the maximum angle of any element exceeds 160° or a liquid-gas interface node reaches the liquid-solid interface. In the later case remeshing is unavoidable since we have to change the boundary description of the node. We implemented the above techniques in the finite element package MooNMD [13].

Remark 3.4.1. Let $X^n(k_{\Gamma_F})$ be a position of a node k on Γ_F which is moving towards Γ_S at time t_n. Let l^n be the gap between $X^n(k_{\Gamma_F})$ and Γ_S in the moving direction of $X^n(k_{\Gamma_F})$. In our computations we change $X^{n+1}(k_{\Gamma_F})$ as $X^{n+1}(k_{\Gamma_S})$ if $(X^{n+1}(k_{\Gamma_F}) - X^n(k_{\Gamma_F})) \geq l^n$ by remeshing the domain. But $(X^{n+1}(k_{\Gamma_F}) - X^n(k_{\Gamma_F}))$ must be less than or equal to l^n since $\mathbf{u} \cdot \nu_S = 0$ on Γ_S and it is called contact condition. The techniques discussed in section 3.2.4 to obtain the new position X^{n+1} may violate the contact condition. To overcome this difficulty we have to use an additional boundary condition as used in elasticity for contact problems [14].

4. Results. In order to validate the model presented in the previous sections, we performed the computations with a variety of parameters. A water droplet of diameter $d_0 = 0.1$ mm was considered to impinge the stationary solid surface with a velocity $\mathbf{u}_0$ = 1 m/sec. For water, the surface tension $\sigma = 0.073$ N/m, density $\rho = 1000\ kg/m^3$, kinematic viscosity $\nu = \mu/\rho = 10^{-6}\ m^2/sec$ were used. The dimensionless values for

the above considered parameters are Re = 100, We = 1.4 and Fr = 1020. We take the friction coefficient term $\frac{\beta}{\rho \mathbf{u}_0} = 10^4$. Figure 4.1 represents the sequence of frames corresponding to the above values in different instances of the impinging process.

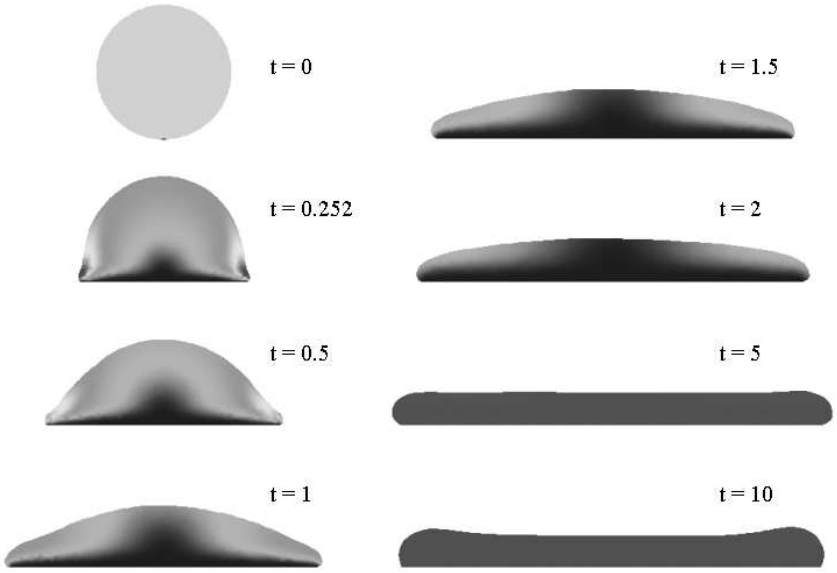

FIG. 4.1. *Water droplet deformation with Re = 100, We = 1.4 and Fr = 1020.*

Figure 4.2 shows the isolines of the first velocity component u_1 in the above spreading process at different instances. Figure 4.3 shows the isolines of the second velocity component u_2.

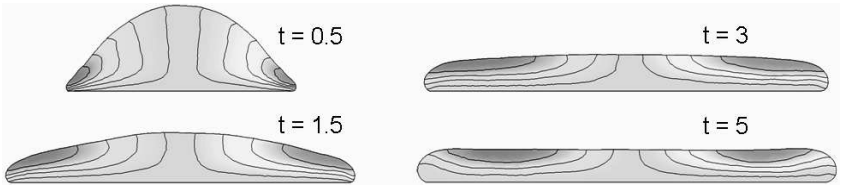

FIG. 4.2. *Isolines of the velocity component* u_1

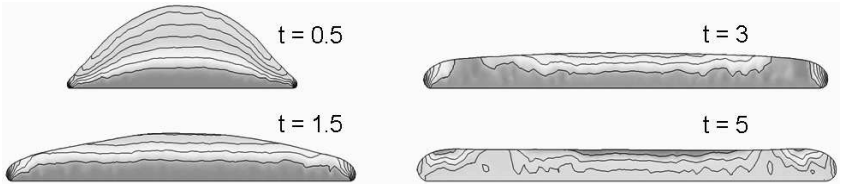

FIG. 4.3. *Isolines of the velocity component* u_2

To study the influence of the impact velocity in spreading process we define the

spreading factor (L) as the ratio between wetting length and initial diameter d_0. Figure 4.4 represents the spreading factors of a water droplet with diameter $d_0 = 0.1$ mm for different impact velocities. In which the wetting length increases if the impact velocity increases. To show the mass conservation of this simulation we define the mass difference factor (E) as the ratio between $meas\Omega(t) - meas\Omega(0)$ and $meas\Omega(0)$. Figure 4.5 shows the mass conservation of the droplet for different impact velocities.

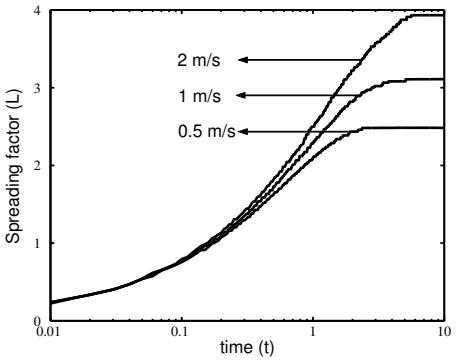

FIG. 4.4. *Spreading factor (L) of the droplet with* $d_0 = 0.1$ *mm,* $\mathbf{u}_0 = 0.5, 1, 2$ *m/s*

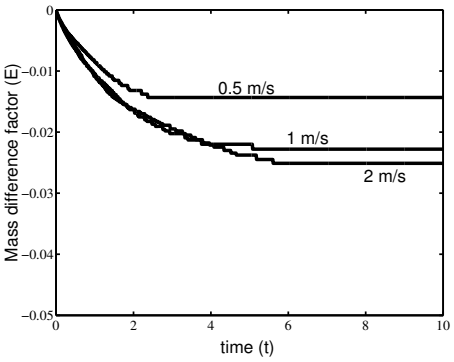

FIG. 4.5. *Mass conservation of the droplet with* $d_0 = 0.1$ *mm,* $\mathbf{u}_0 = 0.5, 1, 2$ *m/s*

Remark 4.1.1. In our model, solid surface properties can be taken into consideration by choosing the friction coefficient β and the contact angle θ. Different formulas for determining the contact angle have been used, in particular a fixed static contact angle of $\theta_{stat} = 105°$ and a dynamic contact angle depending on the tangential velocity near the wetting point. In our first tests we found almost no dependency of the results on the contact angle. A reason may be the d-term in the equation (3.5) dominates the h-term during the spreading process. However, further studies are needed to investigate this phenomenon in more detail.

Acknowledgement. The authors like to thank the Deutsche Forschungsgemeinschaft (DFG) for supporting the research within the graduate program Micro-Macro-Interactions in Structured Media and Particle Systems (GK 828).

REFERENCES

[1] E. Bänsch. *Numerical methods for the instationary Navier-Stokes equations with a free capillary surface.* Habiliationsschrift, Albert-Ludwigs Universität, 2001.
[2] E. Bänsch. Finite element discretization of the Navier-Stokes equations with a free capillary surface. *Numer. Math.*, 88:203–235, 2001.
[3] M. Behr and F. Abraham. Free-surface flow simulations in the presence of inclined walls. *Comp. Meth. in App. Mech. and Engg*, 191(47-48):5467–5483, 2002.
[4] M.O. Bristeau, R. Glowinski and J. Periaux. Numerical methods for the Navier-Stokes equations. Application to the simulation of compressible and incompressible flows. *Comp. Phys.* 6:73–188, 1987.
[5] H.-J. Butt, K. Graf and M. Kappl. *Physics and Chemistry of Interfaces* Weinheim : Wiley-VCH, 2003.
[6] M. Crouzeix and P.-A. Raviart. Conforming and non conforming finite element methods for solving the stationary Stokes equation. *R.A.I.R.O.*, R3:33–76, 1973.
[7] E.B. Dussan V. The moving contact line: the slip boundary condition. *J. Fluid Mech.*, 77(4):665–684, 1976.

[8] J. Eggers and H.A. Stone. Characteristic lengths at moving contact lines for a perfectly wetting fluid: the influence of speed on the dynamic contact angle *J. Fluid Mech.*, 505:309–321, 2004

[9] J. Fukai, Z. Zhao, D. Poulikakos, C.M. Megaridis, and O. Miyatake. Modeling of the deformation of a liquid droplet impinging upon a flat surface. *Phys. Fluid*, A 5(11):2588–2599, 1993.

[10] V. Girault and P.-A. Raviart. *Finite Element Methods for Navier-Stokes equations*. Springer-Verlag, Berlin-Heidelberg-New York, 1986.

[11] L.M. Hocking. A moving fluid interface. Part 2. The removal of the force singularity by a slip flow. *J. Fluid Mech.* 79(2):209–229, 1977.

[12] L.M. Hocking. A moving fluid interface on a rough surface. *J. Fluid Mech.* 76(4):801–817, 1976.

[13] V. John and G. Matthies. MooNMD - a program package based on mapped finite element methods. *Comput. Visual. Sci.*, 6:163–170, 2004.

[14] N. Kikuchi and J.T. Oden. *Contact Problems in Elasticity: A Study of Variational Inequalities and Finite Element Methods* . SIAM Philadelphia, 1998.

[15] G. Matthies. *Finite element methods for free boundary value problems with capillary surfaces*. PhD thesis, Otto-von-Guericke-Universität Magdeburg, Fakultät für Mathematik, 2002.

[16] F. Nobile. *Numerical Approximation of Fluid-Structure Interaction Problems with Application to Haemodynamics*. PhD thesis, École Polytechnique Fédérale de Lausanne, 2001.

[17] R. Rannacher. Finite element methods for the incompressible Navier-Stokes equations. In: Fundamental directions in mathematical fluid mechanics, ed. by Galdi, Giovanni P. et al., *Birkhäuser*, pages 191–293, 2000.

[18] J.A. Sethian. *Level Set Methods*. Cambridge University Press, 1996.

[19] W.J. Silliman and L.E. Scriven. Separating flow near static contact line: Slip at wall and shape of a free surface. *J. Comput. Phys.*, 34:287–313, 1980.

[20] A. Thompson and M. Trian. A general boundary condition for liquid flow at solid surfaces. *Nature*, 389:360–362, 1997.

[21] S. Turek. *Efficient solvers for incompressible flow problems. An algorithmic and computational approach*. Springer-Verlag, Berlin, 1999.